Geophys. J. Int. (2004) **158,** 972–982 doi: 10.1111/j.1365-246X.2004.02340.x

Isolated deep earthquakes beneath the North Island of New Zealand

T. Boddington, C. J. Parkin* and D. Gubbins

School of Earth Sciences, University of Leeds, Leeds LS2 9JT, *UK. E-mail: gubbins@earth.leeds.ac.uk*

Accepted 2004 March 25. Received 2004 March 22; in original form 2003 November 10

SUMMARY

Seismicity shallows towards the south along the Tonga–Kermadec–Hikurangi margin, deep and intermediate seismicity being absent altogether in the South Island of New Zealand. Beneath the Taranaki region of the North Island the maximum depth of the main seismicity is 250 km, but very rare events occur directly below at 600 km. These could be associated with a detached slab or a vertical, aseismic continuation of the subducted Pacific Plate. Six small events that occurred in the 1990s were recorded extensively by digital instruments of the New Zealand National Network (NZNN) and temporary deployments. We relocate these events by a joint hypocentre determination (JHD) method and find their focal mechanisms using first motions and relative amplitudes of *P* and *S* arrivals. The earthquakes relocate to a remarkably uniform depth of 603 ± 3 km relative error (±10 km absolute error) in a line 30-km long orientated 40°NE, roughly parallel to the strike of the intermediate-depth seismicity. The only consistent component of the focal mechanisms is the tension axis: all lie close to horizontal and tend to align with the line of hypocentres. We interpret this deep seismic zone as a detached sliver of plate lying horizontally with the same orientation as the main subducted plate above. Volume change caused by a phase change controlled by the pressure at 600 km and temperature in the sliver produces a pattern of strain that places the sliver under tension along its length.

Key words: deep-focus detached earthquakes, focal mechanism, Hikurangi, New Zealand, relocation, subduction.

1 INTRODUCTION

New Zealand lies over a portion of the Hikurangi margin where the Pacific Plate is being subducted under the Australian Plate (Fig. 1). The Hikurangi margin is part of the Tonga–Kermadec–Hikurangi subduction zone extending northwards into the Pacific Ocean. The rate of subduction is greater in the northeast and diminishes in the southwest to zero near Kaikoura, on the east coast of the South Island. Thus, there is a relative rotation of the two plates of some 7° Myr and palaeomagnetic data show that a finite rotation of at least 60° has occurred in the last 25 Myr (Walcott 1987). The instantaneous rotation pole and the rate of rotation seem to have remained constant from 43 Myr until 10–21 Myr, since which time the pole has begun to move southeastwards away from New Zealand and the rate of rotation has increased.

Further to the southwest the Australian Plate subducts under the Pacific Plate. The Fjordland district in the southwest of the South Island, New Zealand, lies above a near-vertical zone of deep earthquakes. Between these two subduction zones is a region of high shear strain extending along most of the South Island and dissecting the North Island from north to south. Walcott (1987) cites triangulation studies that indicate constant strain rates in the transcurrent and Alpine fault zones of the North and the South islands. To the north, subduction at the Hikurangi margin becomes increasingly oblique towards its southern termination.

The maximum depth of the seismicity shallows progressively from the Tonga end of the plate boundary in the north to the Hikurangi margin in the south. The classic explanation for this, given by McKenzie (1970), was that a subducting plate warms and becomes ductile and aseismic at a progressively shallow depth towards the south, where the convergence rate is lower and the plate takes longer to reach a given depth. By 39°S the seismicity extends to a depth of only 250 km, but a small number of very deep events occur directly beneath those at 250 km (Fig. 2). Some of these deep events are apparent in the original paper of McKenzie (1970); they were discussed first by Adams (1963). This cluster is clearly isolated from the main seismicity. Similar isolated clusters of deep events occur elsewhere (Lundgren & Giardini 1994; Okal 2001).

The first recorded isolated deep event under New Zealand was in 1953 at 570-km depth, followed by two events in 1960 at 607 and 612 km, occurring just five minutes apart (Adams 1963). Adams tentatively proposed a focal mechanism for the 1960 deep event. The data were inadequate to establish a mechanism by first motions, so instead he noted that most of the observed first motions were opposite in sense to those of a twin intermediate-depth event at

*Now at: Bullard Laboratories, Department of Earth Sciences, University of Cambridge, Madingley Road, Cambridge CB3 0EZ, UK.

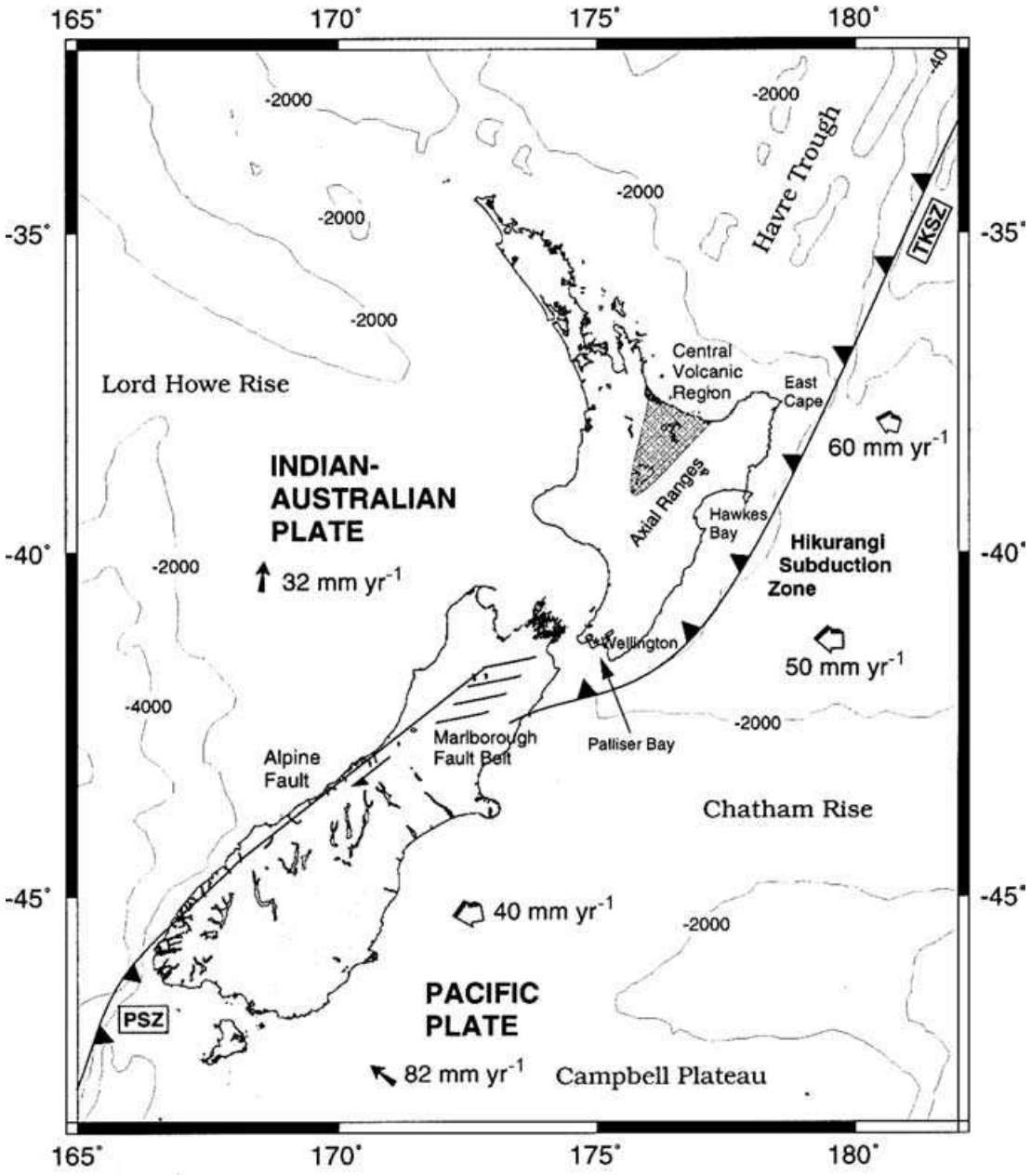

Figure 1. Plate configuration and major tectonic features of the convergent margin of New Zealand. Convergence rates are indicated by open arrows (Walcott 1978) and absolute plate motions by solid arrows (Minister & Jordan 1978). Bathymetry contours are in metres. The Hikurangi margin is the southwestern continuation of the Tonga–Kermadec subduction zone (TKSZ). After Brisbourne (1998).

228-km depth that occurred some five days later with the same epicentre. A focal mechanism was determined for the intermediate-depth event, so the data for the deep event are consistent with a mechanism of similar orientation but with the pressure and tension axes transposed. This focal mechanism is sometimes referred to as a full solution (e.g. Okal 2001), but this is not what was originally intended.

A further deep-focus earthquake took place in 1975 (Adams & Ferris 1976) at 582-km depth. First-motion observations were consistent with the earlier deep events, but again were insufficient to give a fault-plane solution. At four New Zealand stations above the shallowest part of the seismic zone, converted phases were observed in between the *P* and *S* phases. These were attributed to *SP* conversions at depths consistent with the bottom of the main seismic zone. Because the deep earthquakes take place directly below the end of the Wadati–Benioff zone, rather than on a projection of that zone, Adams & Ferris (1976) concluded that they originate in a detached slab of subducted lithosphere and that the converted phases were the result of a sharp discontinuity representing the bottom of the main subducting slab.

Six deep events were recorded in the 1990s beneath Mount Taranaki (formerly Mount Egmont), North Island, close to the epicentres of the earlier deep earthquakes, and are the subject of this study. They are smaller than the earlier earthquakes and occurred when a large number of modern, digital seismometers were in operation in New Zealand. These have provided an excellent data set for this study, although the geographical coverage is not better than in 1960.

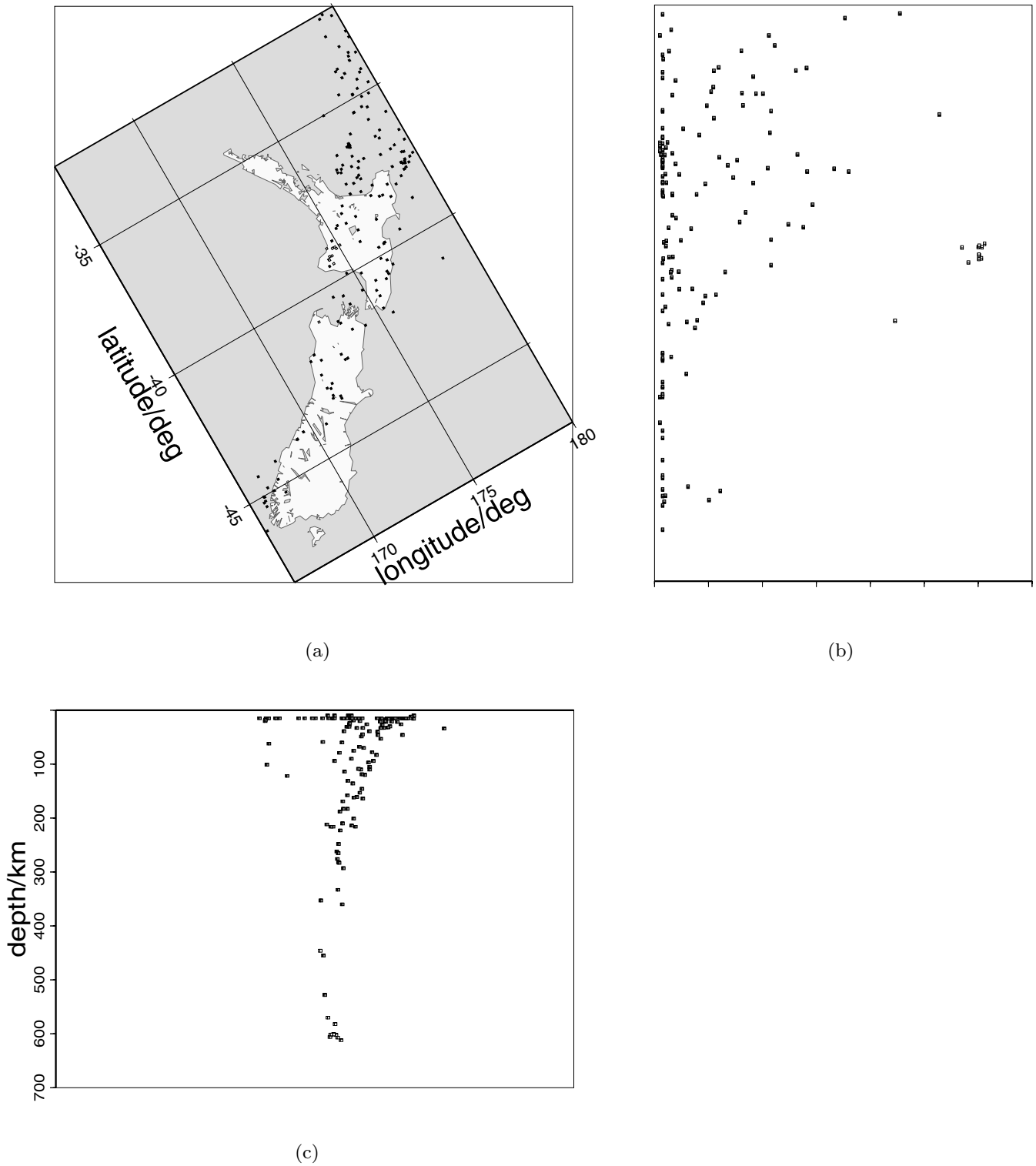

Figure 2. Seismicity of the Hikurangi subduction zone. Data: Adams (1963) and Adams & Ferris (1976); ISC (2003, NZ deep events, unfilled squares), Harvard Centroid Moment Tensor Catalog (other events, filled squares). The vertical scale is twice the horizontal. (a) Plan view, with viewpoint at 210°. (b) Elevation perpendicular to the strike of the subduction zone (viewpoint at 120°), showing a decrease in the maximum depth of the Wadati–Benioff zone to the southwest. (c) Elevation parallel to the strike of the subduction zone (viewpoint at 210°) showing the double seismic zone of the steeply dipping plate and volcanic seismicity beyond the subduction zone. The deep events under western North Island clearly comprise an isolated cluster.

The main reason to study these isolated deep clusters of events is to establish whether they are truly detached, and are part of an isolated piece of subducted lithosphere, or whether the subducted plate is aseismic at intermediate depths. Okal (2001) has reviewed this and other clusters that are isolated from the main seismically active part of their subduction zones. Using the spectral ratio technique, he estimates Q_μ at approximately 300 for the 1992 July 8 and 1998 July 4 events. This is very much lower than in other

subduction zones and suggestive to Okal (2001) of a discontinuity in the cold subducted material. It is consistent with a slab that ends, along with seismicity, at approximately 200-km depth with $Q_\mu \approx 800$ and 400 km of mantle with a tentative value of $Q_\mu \approx 250$. This depth is consistent with the converted phases noted by Adams & Ferris (1976), but whereas they interpreted them as *SP* conversions, Okal suggests they could be *PS*, with conversion occurring near the end of the slab at some 200-km depth. However, he concedes that an internal reflection provides an alternative explanation and notes that such phases have been observed at Global Digital Seismic Network (GDSN) station SNZO from earthquakes at intermediate depths, where there is certainly continuous high-Q material between the hypocentre and the receiver. *PS* is difficult to identify with the vertical component stations that were available in 1975.

Various tomographic studies (van der Hilst 1995; van der Hilst & Snieder 1996) have revealed high seismic velocity anomalies associated with subducting slabs in the western Pacific that are continuous through aseismic zones. Some also show horizontal deflections of the Izu–Bonin (van der Hilst *et al.* 1991), Honshu and southern Kuril (Fukao *et al.* 1992) and northern Tonga (van der Hilst 1995) slabs at the 670-km discontinuity, suggesting that even the outboard events in the Tonga subduction zone take place within a continuation of the slab; however, they appear to show a gap in the velocity anomaly in the region of the North Island, New Zealand (van der Hilst *et al.* 1991; van der Hilst 1995), suggesting the deep seismicity there may lie within a detached piece of subducted plate.

2 DATA

This study used arrival times, polarities, relative amplitudes and polarizations from a range of permanent and temporary stations in the New Zealand region. The New Zealand National Network (NZNN), operated by the Institute of Geological and Nuclear Sciences (IGNS) of New Zealand, provided the largest number of stations (Fig. 3a). It provides good coverage of the territory of New Zealand, but the instruments are short-period and the majority are vertical-component. Usually approximately 10 three-component recordings were available for each event.

The portable broad-band array POMS I of Leeds University (Fig. 3b) was in place for the events of 1991 September 14, 1992 February 26 and 1992 July 8; the POMS II broad-band array for that of 1994 April 8. The seismometers were Guralp CMG-3T three-component seismometers with RefTek recorders. As well as providing broad-band records, POMS I was a dense array with 10-km station spacing that provided control on short-wavelength variations in the waveforms caused by local anomalies in structure (Stuart *et al.* 1994).

The PANDA II array was part of a deployment by Memphis State University in 1994 (Fig. 3b). This network had the advantage of being directly above the source region. The network lost all timing early on in the experiment and all instruments drifted away from UTC. As a result no absolute timing could be used, but waveforms and relative timing across the array could be used because data were telemetered to a central clock.

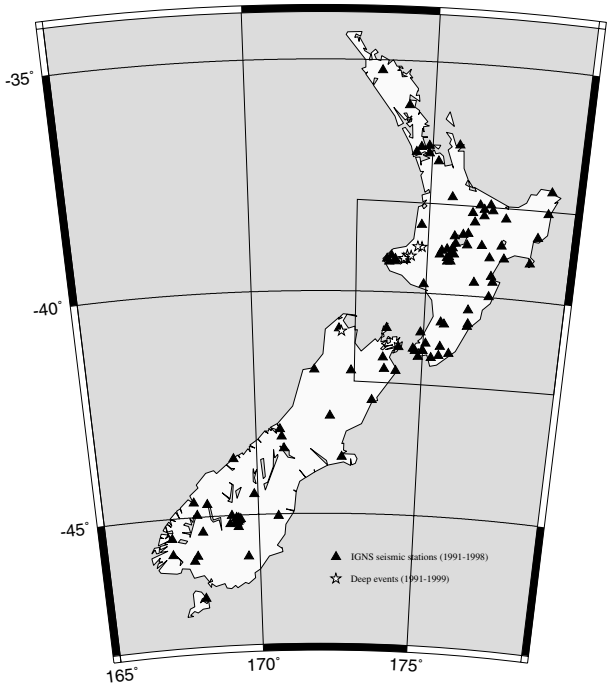

(a) Stations of the IGNS on 1994/April/08 (triangles). Most are single-component. The deep Taranaki events are also shown (stars).

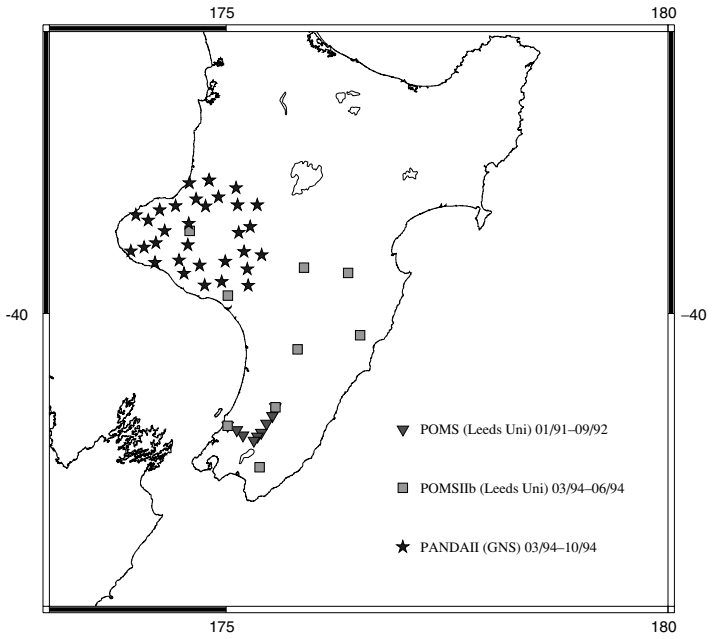

(b) Temporary portable networks used in this study.

Figure 3. Geographical coverage of seismic stations.

Two of the events were recorded globally. Data from a small number of GDSN stations were used.

It is important to verify the polarity and convention of each station when using first motions. POMS I polarities were checked using teleseisms with known source mechanisms published in the Harvard CMT Catalog. The POMS I and II deployments used different recorders, which in turn used different conventions, but were consistent. A considerable number of NZNN stations have reversed polarity. The true polarity of most of these, and of the horizontal components in a few cases, were supplied by M. Reyners of IGNS (Reyners, private communication 2002). Picks at some NZNN stations for which the directions of the vertical components were not known had to be discarded. Similarly, the directions of horizontal components at NZNN stations were inconsistent and were deduced from those of the vertical components using the *P*-wave first motions.

Fig. 4 shows seismograms of the 1991 event from station LTW2 of the POMS I array, located in the Wairarapa valley southeast of the epicentre. This broad-band record has been high-pass filtered above 1.5 Hz to remove microseismic noise. The *P* wave and its first motion are easily read, but there is significant energy on the transverse component indicating lateral variations in structure along the path. The *P*-wave train contains a large amount of high-frequency energy in the range 5–10 Hz, indicating a high-*Q* path from the event to the station. The *S* wave is preceded by an *SP* conversion that is most clearly visible on the vertical component (Fig. 4c). Some energy also arrives on the transverse component: this is probably a result of out-of-plane propagation in the highly anomalous region beneath the station. This conversion is from the top of the subducted plate, which is approximately 20 km below the station. The polarity is linear for the first 2 s of the *S* wave, from 135 s on the plot, but it deteriorates after 137 s. Fig. 5 shows seismograms from the same event at station WLZ of the NZNN, located near Hamilton. This *S* wave appears to have a consistent polarity throughout but in fact the plane of polarization rotates through nearly 90° at 136 s, after which the energy is confined to the north component. This is another example of multipathing, probably again caused by refraction at the top of the subducted Pacific Plate.

The high-frequency nature of the seismograms and frequent multipathing preclude the use of any sophisticated waveform-modelling methods for finding the focal mechanism: such methods would require an impossibly detailed 3-D model of the structure. We have therefore concentrated on first motions and amplitude ratios.

All traveltimes and *P*-wave polarities were picked by the authors except for a small number of teleseisms reported by the International Seismological Centre (ISC). Time picks were weighted according to the convention in the relocation program described in the next section.

3 METHODOLOGY

3.1 Locations

Each of the six Taranaki events studied here has been located by the ISC (Table 1). All registered a body wave magnitude (m_b) less than 5.0. Global coverage is poor and only the two largest events, 1991 and 1998, were recorded at distances beyond the South Pole.

Ideally, the depth of deep hypocentres is constrained by the relative timing between the direct *P* arrival and later *pP* phase. No surface reflections have been recorded for these events. However, as noted by Okal (2001), the depth of these events is very well controlled by regional stations, typical formal errors being less than 20 km (Table 1).

The cluster of events in the nineties is ideally suited to refinement by the joint hypocentre determination (JHD) method of Douglas (1967): it occupies a volume a few tens of kilometres across and regional station coverage is excellent. Many stations record most of the events. We used the version of the method described by Pujol (1988, 2000). The program is available from the Orfeus web site `http://orfeus.knmi.nl`.

JHD finds source locations and station corrections simultaneously. Each station–phase combination has its own constant correction, independent of azimuth, that takes account of lateral variations in structure. Where the events form a relatively tight cluster, this improves the quality of the relocations as well as providing information about the local velocity structure. Henceforth, station in this context will be taken to mean station–phase.

The 1991 event was the most widely recorded teleseismically and therefore has the best absolute location (Table 1). Other events may be located relative to this master. The relative locations are more accurate than the absolute location of the master and the absolute location of each event is likely to be limited in accuracy by that of the master. The use of a master event replaces teleseismic information, so only regional stations were used in the JHD relocation. This in turn allowed a flat-earth approximation for the velocity structure. We used the layered structure shown in Table 2, which is known to be a good 1-D approximation to the structure beneath the North Island.

Relocation is an iterative process starting from an initial set of event locations and station corrections. We started from the ISC locations shown in Table 1 and zero for all station corrections. The sum of station corrections remains undetermined at each iteration because a single delay in all origin times produces the same delay at all stations. This delay is set to zero at each iteration by removing the corresponding eigenvector when calculating the generalized inverse of the condition matrix. The sum of station corrections provides a check of the numerical accuracy of the method.

The station corrections obtained are shown in Fig. 6 using Delaunay triangulation, but excluding stations that recorded fewer than three events. Their largest absolute values just exceed 1.0 s. In the North Island, arrivals are early in the northeast and late both in the south and near Mt Taranaki in the west. This is consistent with waves passing through the fast, subducted Pacific Plate, to stations in the north and east, and through the slow wedge above the slab towards stations further west. Station corrections in the South Island show a trend from slow in the northwest to fast in the southeast.

Station corrections were also calculated using IASP91 traveltime tables and the original locations. In the North Island the pattern of station corrections was similar but in the South Island it was reversed, with the trend from northwest to southeast being from fast to slow. This is attributed to relocation and strong lateral variations in the source region.

JHD gives error estimates on the relative location of each event assuming the data set has the resolution to decouple the station corrections from the locations. We studied the covariance matrices for each of the six events. These show the origin times to be best determined, followed by the latitude, depth and longitude. An inspection of the eigenvectors of the covariance matrices shows the epicentres have least uncertainty roughly along the strike of the country. This is to be expected because the stations are all on land and are therefore aligned with the country; the coverage is good in that direction but poor across the country.

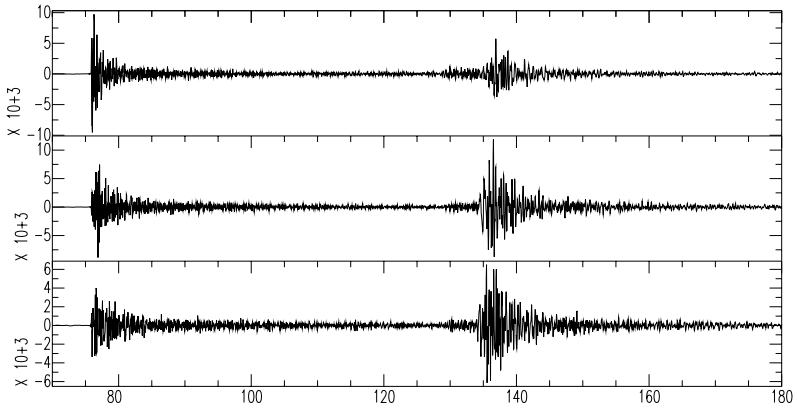

(a) Full seismogram

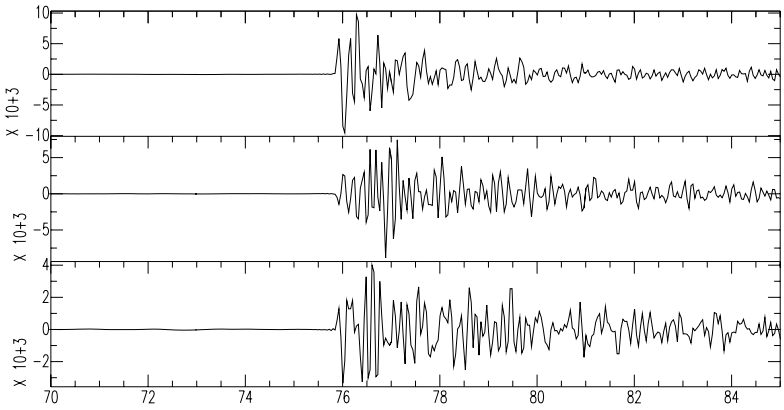

(b) Close-up of P arrival

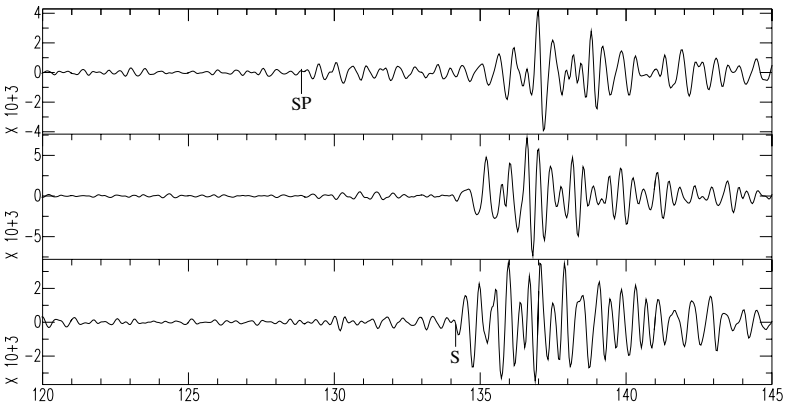

(c) Detail of S arrival

Figure 4. Seismograms of the 1991 event recorded at station LTW2. Components are vertical (down), radial, transverse.

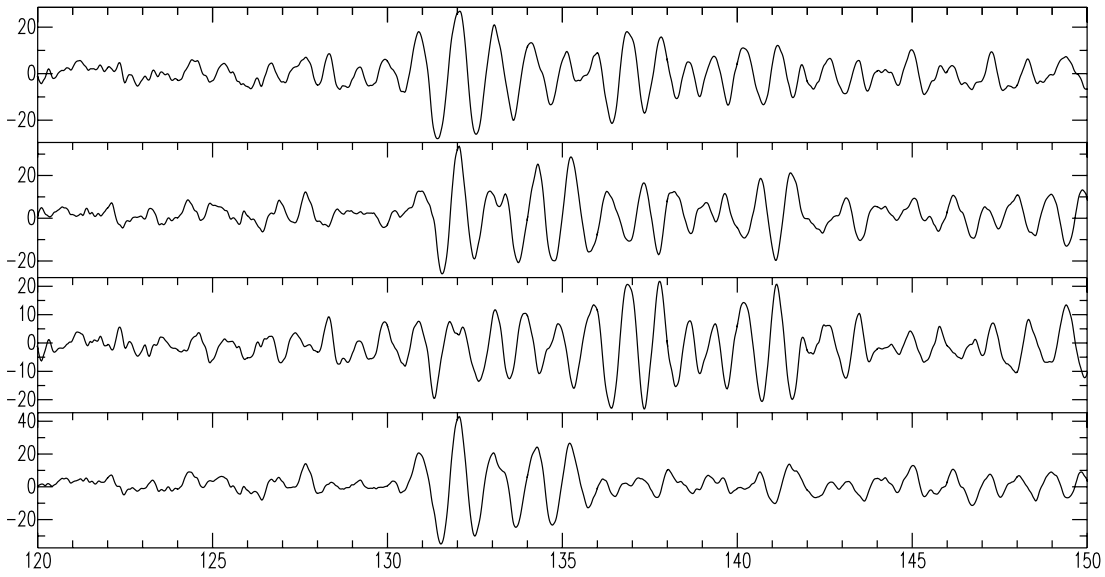

Figure 5. Seismograms of the 1991 event recorded at station WLZ. The shear wave is shown; components are radial, transverse, north, east.

Table 1. New Zealand deep events.

Date	Magnitude	Latitude	Longitude	Depth/km	Source
1953/03/24	$M_L = 4.5$ –5.25	−38.9°	174.5°	570	Adams (1963)
1960/03/23	$M_L = 6.25$	−39° 03′ ± 04′	174° 52′ ± 08′	607 ± 4	Adams (1963)
1960/03/23	$M_L = 6.2$	−39° 06′ ± 07′	175° 04′ ± 12′	612 ± 9	Adams (1963)
1975/02/07	$M_L = 4.9$	−39.27° ± 0.06°	174.26° ± 0.08°	582 ± 7	Adams & Ferris (1976)
1991/09/14	$m_b = 4.8$	−39.18° ± 0.067	174.4° ± 0.15°	602 ± 8.4	ISC
1992/02/26	$m_b = 4.0$	−38.90° ± 0.170°	174.7° ± 0.34°	602.1 ± 21.9	ISC
1992/07/08	$M_L = 4.9$	−39.10° ± 0.150°	174.4° ± 0.24°	622.3 ± 26.9	ISC
1993/05/05	$M_L = 4.6$	−38.90° ± 0.160°	174.4° ± 0.20°	577	ISC
1994/04/08	$m_b = 3.8$	−39.19° ± 0.072°	174.5° ± 0.16°	601.6 ± 9.4	ISC
1998/07/04	$m_b = 4.2$	−39.26° ± 0.065°	174.5° ± 0.12°	601.7 ± 4.8	ISC

Table 2. Velocity Model used in JHD program.

Depth (km)	V_P	V_P/V_S
0	5.5	1.666
12.0	6.5	1.757
33.0	8.1	1.761
250.0	8.8	1.858
400.0	9.7	1.849
650.0	10.5	1.826

Table 3 gives the semi-axes of the relative error ellipsoid for each event, calculated from the square roots of the eigenvalues of the covariance matrix. Origin time is not included as this is typically much better determined than any of the three space coordinates (in the sense that the error in the origin time multiplied by the seismic velocity at the source is much less than the error in any one of the spatial coordinates). The eigenvectors give the orientation of each of the axes. These are not shown, but for all events they are roughly oriented perpendicular to the strike of the country and 20° to the horizontal (denoted 1), along strike and down 30° (denoted 2) and 55° down (denoted 3). Roughly speaking, one standard deviation in latitude, longitude and depth is 0.5 km, 2 km and 1 km, respectively.

3.2 Focal mechanisms

We found focal mechanisms for the six events using first motions of *P* and *S* supplemented by amplitude ratios of *P*/*SH* and *SH*/*SV* and the FOCMEC program developed by Snoke (2003 `http://www.geol.vt.edu/outreach/vtso/focmec`). The process is accomplished in four stages:

(i) A 1-D reference model is used to calculate the azimuths, take-off angles, emergent angles and traveltimes of *P* and *S* waves travelling from the hypocentres to each station. The reference model used was IASP91 (Kennett & Engdahl 1991).

(ii) A list of codes representing the *P*, *SV* and *SH* polarities and amplitude ratios at each station is matched to the corresponding ray parameters. Any subset of these observations may be used. Amplitudes are read from vertical, radial and transverse components and a free-surface correction is automatically applied based on the V_P/V_S ratio at the surface.

(iii) Double-couple focal mechanisms are sought that are consistent with as many as possible of the observations. The program searches through all possible combinations of the auxiliary and fault planes. The user may specify the number of errors to be allowed in each category of input before a putative solution is discarded. There is the option to weight each polarity error with a computed radiation factor, because lower amplitude signals near to nodal planes are more prone to incorrect picking. The latter option was not used in this study because of the incomplete coverage of the focal sphere. Because most data came from New Zealand stations with azimuths roughly northeast or southwest, the weighting option would have tended to favour solutions with one nodal plane near to this strike.

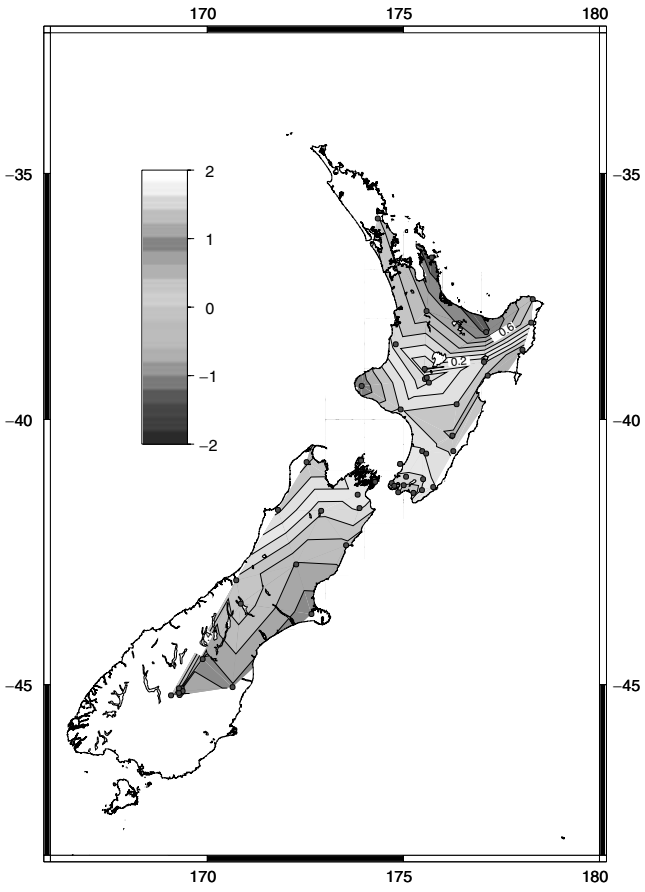

Figure 6. JHD-calculated station corrections. Only stations recording three or more events have been contoured.

Table 3. Errors of relative locations in km (semi-axes of error ellipsoids).

Date	1	2	3
1991/09/14	1.0	0.3	0.5
1992/02/26	2.5	0.9	1.4
1992/07/08	1.9	0.7	0.8
1993/05/05	1.4	0.4	0.7
1994/04/08	1.2	0.5	0.6
1998/07/04	1.8	0.7	1.3

The result is a number of possible solutions and the corresponding numbers of polarities and amplitude ratios that are in error. A trial-and-error approach is required to find an acceptable level of error that produces an acceptable range of solutions.

Where data in different categories are mutually inconsistent, a subjective decision must be taken as to which are the more reliable. *P* polarities may be accorded more confidence than *S* polarities, because *S* first motions tend to be obscured by the tail of the *P* phase and sometimes by *SP* conversions. For the latter reason, *SV* polarities are in turn less reliable than *SH* polarities.

Furthermore, a substantial exercise was undertaken as part of this study to confirm the polarities of horizontal components of the NZNN seismometers. The polarities of the *P* arrivals on the vertical components were used in conjunction with the event-station azimuths to predict their polarities on the horizontal components. The predicted and observed polarities were compared to identify any horizontal components that might be reversed. In practice, reversed components appeared to be mostly confined to the single-component stations, but there remains the possibility that some *S* polarities were incorrect as a result of reversed instrument polarities, making this category of data less reliable than the *P* polarities.

P-wave first motions were picked from vertical components alone, although in rare cases the other components helped to identify the first arrival. Butterworth high-pass filters were used to filter out long-period noise in many cases, because New Zealand is subject to high-amplitude microseismicity that dwarfs the signals of the events studied at some stations. The cut-off frequency was chosen according to the data; typically a frequency of 0.5–1.0 Hz was used. In rare cases where an examination of the noise spectrum revealed high-frequency noise, a low-pass filter at 10–15 Hz was applied. A small number of additional *P*-wave first motions from the ISC were particularly helpful in constraining some of the solutions, because they mostly referred to stations outside New Zealand and covered a different part of the focal sphere.

First motions of *S* phases were picked at three-component stations that comprised a subset of those used for the *P* phases. Of these, not all could be used because the polarities of the horizontal components of some instruments could not be verified. In order to facilitate picking, components were rotated using the *P*-wave parameters to *P*, *SV* and *SH*, respectively. Some first motions were very clean and could easily be picked from a single component. The correlation between the *SV* and *SH* (transverse) components was often used to assist picking. Comparison with the longitudinal component was occasionally helpful in distinguishing genuine *S* arrivals from *SP* conversions.

SH/*P* amplitude ratios were picked for three of the six events whose mechanisms could not be constrained using polarities alone. Like the first-motion polarities, these amplitudes were picked from the seismograms by eye. They were only used where they could be clearly read from the very first motions of each arrival and then only when these were of similar duration (Julian, private communication, 2003).

For the event of 1992 February 26, *SV*/*SH* amplitude ratios were obtained by polarization analysis of three-component seismograms in the time domain, taking successive time intervals (typically 0.5 or 1.0 s) in increments of half that interval. Linear polarization, when it was observed, was usually confined to the first 2 s of the *S*-wave train. This method gave an amplitude ratio even when it was impossible to determine the first motion. Twelve amplitude ratios were obtained for this event, but they failed to discriminate between our preferred and secondary solutions described above.

4 RESULTS

4.1 Locations

The hypocentres and source times determined using JHD are listed in Table 4. The relocated events lie between 600 and 606 km and define a remarkably horizontal plane. The depth error is at most

Table 4. Relocated events.

Event	Latitude	Longitude	Depth
1991/09/14	−39.180	174.430	602.0
1992/02/26	−38.987	174.833	602.2
1992/07/08	−39.277	174.350	601.3
1993/05/05	−38.981	174.714	600.2
1994/04/08	−39.192	174.541	601.3
1998/07/04	−39.250	174.335	606.0

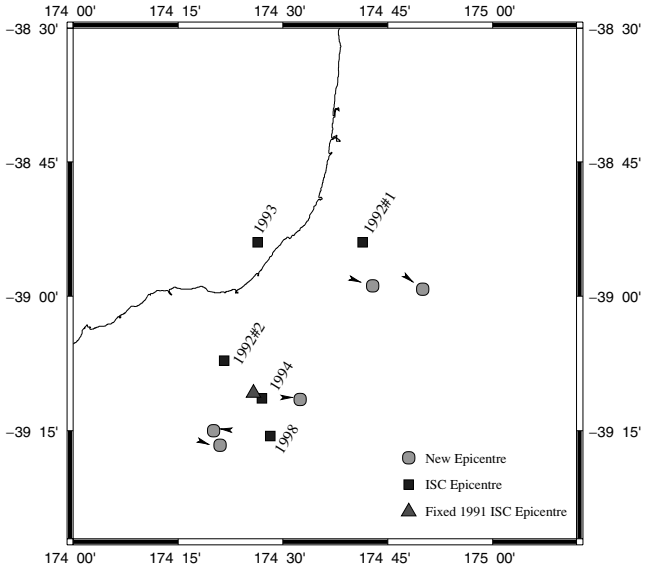

(a) Plan

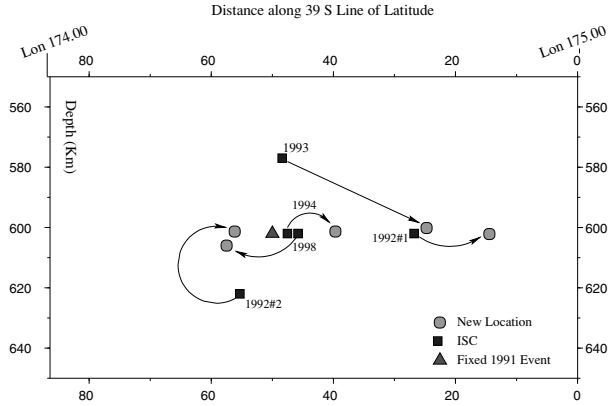

(b) Elevation

Figure 7. Relocations from ISC hypocentres. Arrows indicate movement to new locations. The 1991 September 14 master event is indicated by the triangle and is still in its ISC-determined position. Other ISC positions are represented by squares and new positions by circles. Units are km.

±2 km (Table 3). Figs 7(a) and (b) show the events in plan and section view. The absolute depths of the events are tied to the ISC location of the 1991 September 14 master event ± 8.4 km. The depths are consistent with those of the four earlier events studied by Adams & Ferris (1976, Table 1), suggesting that all of the deep seismicity occurs at essentially the same depth.

The plan view of Fig. 7(a) suggests that the events are aligned roughly along the strike of both the plate boundary and the shallower seismicity, with azimuth 040°. The deep seismic zone extends 30 km in this direction: a remarkable straight, level feature.

4.2 Mechanisms

The *P*, *SV* and *SH* polarities were not always mutually consistent. In general, the *SV* polarities were inconsistent with the mechanisms determined using the more reliable *P* and *SH* polarities and amplitude ratios. The six focal mechanisms are given in Table 5 and Fig. 8.

Table 5. Summary of the fault-plane solutions determined in this study.

Date	Solution		
	Dip	Strike	Rake
1991/09/14	68° ± 1°	123° ± 3°	−40° ± 6°
1992/02/26	50° ± 2°	236° ± 1°	−57° ± 6°
1992/07/08	66°	143°	−51°
1993/05/05	67°	4°	20°
1994/04/08	35° ± 5°	296° ± 5°	−11° ± 6°
1998/07/04	38°	6°	−47°

Because the software used performs a grid search of the solution space, rather than an inversion, it does not return error bounds. In some cases, however, a group of similar solutions was returned, rather than a single solution, giving some indication of the accuracy of the solutions. The ranges of solutions returned are indicated in Table 5 where applicable.

Of greater importance is the existence of quite different solutions with greater, but still relatively small, numbers of errors. These are analogous to the secondary minima encountered in minimum-norm inverse problems, but here the discrimination of solutions is subjective because there is no objective way to weight the various categories of data used. Of the six events studied, only that of 1992 February 26 had a plausible alternative mechanism to that published here, namely: dip = 35°, strike = 260°, rake = −90°.

The main consistency between these mechanisms lies with the tension axes, which are predominantly horizontal and tend to point along the strike of the seismicity (Fig. 9b). This also applies to our alternative mechanism for the 1992 February 26 event. The mean tension axes of all the events lies 20° up from the horizontal with azimuth 009°. Pressure axes are more scattered, although there is a rough trend for them to be contained in a steeply inclined layer extending NW–SE. Both fault and auxiliary planes are scattered.

5 DISCUSSION

The main evidence for continuity of plate through an aseismic zone, such as may exist here between 250- and 600-km depth, is the existence of a fast, high-*Q* path from the events to some of the stations. We have not found any evidence of high seismic velocity, in agreement with tomographic studies (e.g. van der Hilst 1995), but we do observe very high frequency arrivals (Fig. 4). This high-frequency content points to a high-*Q* path in the mantle. It could be evidence of an aseismic subducted slab, but it is also possible that high frequencies propagate through the lower part of the upper mantle and it is only low *Q* in the asthenosphere and upper reaches of the mantle that cause the usual removal of high-frequency energy. Many stations in the North Island, New Zealand, lie a short distance above the subducted Pacific Plate and enjoy a high-*Q* path through the asthenosphere. The high-frequency content of many arrivals is not therefore incontrovertible evidence of a high-*Q* path below 250-km depth.

Subduction zones that continue from the surface to the bottom of the upper mantle exhibit stronger seismicity at the bottom than at intermediate depths. Perhaps this slab, with its very slow subduction rate, shows an extreme form of this with rare deep earthquakes and very rare events at intermediate depth, so rare as to be non-existent on the historical timescale. The change in seismicity at 250 km seems too abrupt for this, but the implicit change in dip of the slab

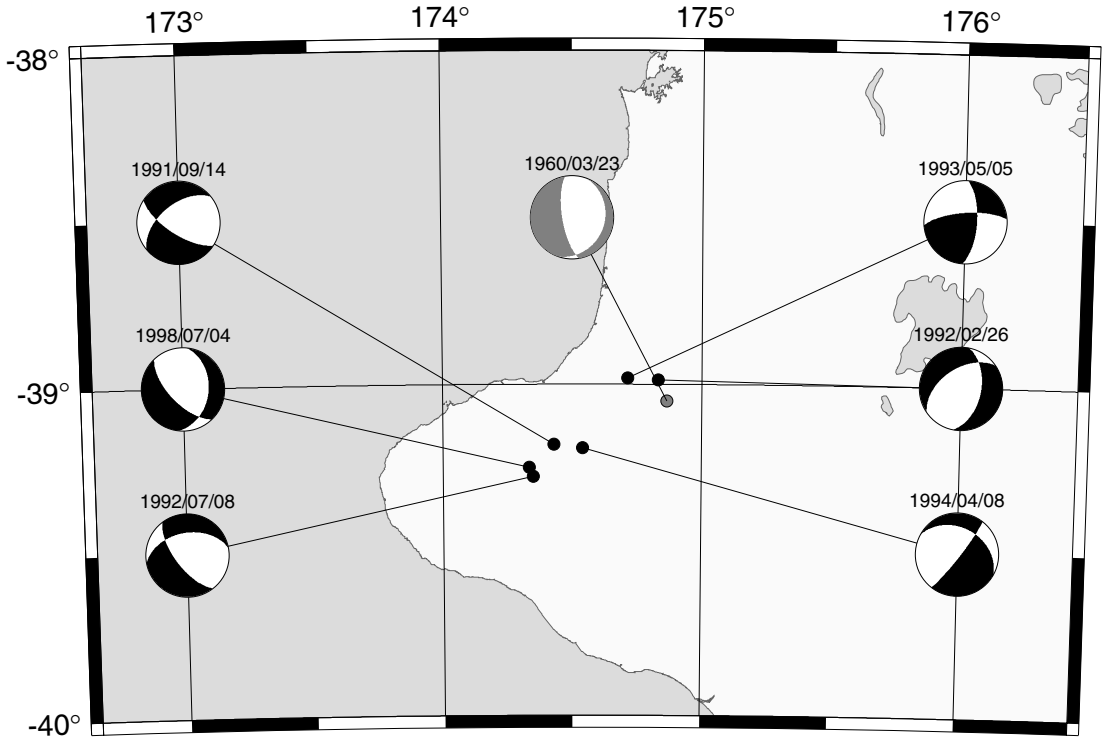

Figure 8. Locations and focal mechanisms of the 1990s Taranaki deep events. The grey shaded event is that of Adams (1963).

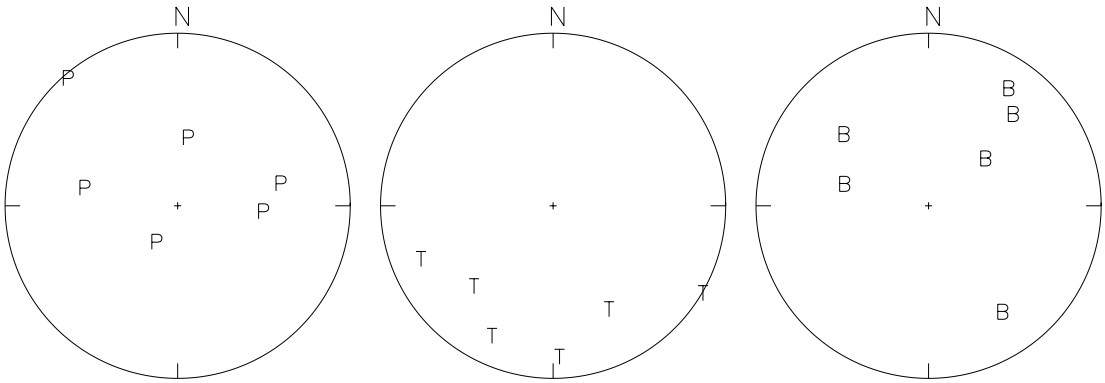

(a) Pressure. (b) Tension. (c) Null.

Figure 9. Pressure, tension and null axes of the six events, plotted on the lower focal hemisphere.

to near-vertical at this depth could result from a change in relative plate motion in the past and consequent change in vertical descent rate of the aseismic part of the slab. The earthquakes studied here are aligned with the strike of the shallower seismicity, which is suggestive of a connection with the events higher up.

If the deepest seismicity is caused by resistance at a phase boundary, we expect the *P* axes of the focal mechanisms to be predominantly vertical. Okal (2001) uses this as a test for mechanical integrity of a slab. This is not the case with our focal mechanisms (Fig. 9a). If the subducted plate is prevented from passing into the lower mantle and spreads out along a horizontal surface, we would expect the state of stress to favour fractures with tension axes horizontal but along the direction of movement of the plate. This is not observed here: the tension axes align along the strike of the seismicity. A NW–SE layer of metastable olivine in a matrix of transformed spinel could produce a self-stress with in-plane *P* axes (Kirby *et al.* 1991, 1996). This could explain the rough trend of the *P* axes we find.

The most remarkable observation we have made is the consistent depths of these events, ± 2 km, over a longer horizontal distance of 30 km. This suggests pressure control of the phase change causing the activity and a rather static piece of slab material, one lying on a constant-density surface that is not descending rapidly. Volume reduction of the phase change would produce a state of stress within the slab fragment that dominates the style of focal mechanism, giving predominantly normal faulting. If the slab fragment is elongated along strike and horizontally, as the seismicity suggests, the tension axes would also be along strike and horizontal, as is observed. Other components of the focal mechanisms are determined by the random fault orientations within the slab fragment.

A similar situation of a recumbent piece of slab was deduced by Okal & Kirby (1998) for deep Fiji events, but they found more scatter

in depth and total scatter in focal mechanisms. Their events were at 660 km whereas ours are shallower. No known phase change occurs within 20 km of 600 km, the absolute depth of these earthquakes within the likely error. We must therefore appeal to a delayed phase change in metastable olivine.

The most plausible explanation of these exceptional deep earthquakes is therefore volume contraction within a small, detached slab fragment lying horizontally at an azimuth of 040°.

ACKNOWLEDGMENTS

The authors would like to thank Martin Reyners, Wei-Jian Mao, Steve Kirby, Bruce Julian and the editors and reviewers Rob van der Hilst, Robin Adams and Emile Okal for their advice. TB was supported by a NERC studentship and CJP by the Isle of Man Board of Education.

REFERENCES

Adams, R.D., 1963. Source characteristics of some deep New Zealand earthquakes, *New Zealand Journal of Geology and Geophysics,* **6**(2), 209–220.

Adams, R.D. & Ferris, B.G., 1976. A further earthquake at exceptional depth beneath New Zealand, *New Zealand Journal of Geology and Geophysics,* **19**(2), 269–273.

Brisbourne, A.M., 1998. Shear-wave structure of the Hikurangi subduction zone, North Island, New Zealand, *PhD thesis,* School of Earth Sciences, University of Leeds, UK.

Douglas, A., 1967. Joint epicentre determination, *Nature,* **215,** 47–48.

Fukao, Y., Obayashi, M., Inoue, H. & Nenbai, M., 1992. Subducting slabs stagnant in the mantle transition zone, *J. geophys. Res.,* **97,** 4809–4822.

Harvard Centroid Moment Tensor Catalog, 2003. `http://www.seismology.harvard.edu/CMTsearch.html`.

ISC, 2003. International Seismological Centre, On-line Bulletin, `http://www.isc.ac.uk/Bull`., International Seismological Centre, Thatcham, UK, 2003.

Kennett, B.L.N. & Engdahl, E.R., 1991. Traveltimes for global earthquake location and phase identification, *Geophys. J. Int.,* **122,** 429–465.

Kirby, S.H., Durham, W.B. & Stern, L.A., 1991. Mantle phase-changes and deep-earthquake faulting in subducting lithosphere, *Science,* **252,** 216–225.

Kirby, S.H., Stein, S., Okal, E.A. & Rubie, D.C., 1996. Metastable mantle phase transformations and deep earthquakes in subducting oceanic lithosphere, *Rev. Geophys.,* **34,** 261–306.

Lundgren, P. & Giardini, D., 1994. Isolated deep earthquakes and the fate of subduction in the mantle, *J. geophys. Res.,* **99,** 15 833–15 842.

McKenzie, D.P., 1970. Temperature and potential temperature beneath island arcs, *Tectonophysics,* **10**(1–3), 357–366.

Minister, J. & Jordan, T., 1978. Present-day plate motions, *J. geophys. Res.,* **83,** 5331–5354.

Okal, E.A., 2001. 'Detached' deep earthquakes: are they really?, *Phys. Earth planet. Int.,* **127,** 109–143.

Okal, E.A. & Kirby, S.H., 1998. Deep earthquakes beneath the fiji basin, sw pacific: Earth's most intense deep seismicity in stagnant slabs, *Phys. Earth planet. Int.,* **109,** 25–63.

Pujol, J., 1988. Comments on the joint determination of hypocenters and station corrections, *Bull. seism. Soc. Am.,* **78**(3), 1179–1189.

Pujol, J., 2000. Joint event location—the JHD technique and applications to data from local seismic networks, in *Advances in seismic event location,* Modern approaches in geophysics Vol. 18, pp. 163–204, eds Thurber, C.H. & Rabinowitz, N., Kluwer Academic Publishers, Dordrecht, the Netherlands.

Snoke, J.A., 2003. FOCMEC: FOCal MEChanism determinations, in *International Handbook of Earthquake and Engineering Seismology,* eds Lee, W.H.K. *et al.,* Academic Press, San Diego, pp. 1629–1630.

Stuart, G.W., Francis, D., Gubbins, D. & Smith, G., 1994. Tararua broadband array, North Island, New Zealand, *Bull. seism. Soc. Am.,* **85,** 325–333.

van der Hilst, R., Engdahl, E.R., Spakman, W. & Nolet, G., 1991. Tomographic imaging of subducted lithosphere below northwest Pacific island arcs, *Nature,* **353,** 37–43.

van der Hilst, R.D., 1995. Complex morphology of subducted lithosphere in the mantle beneath the Tonga trench, *Nature,* **374,** 154–157.

van der Hilst, R.D. & Snieder, R., 1996. High-frequency precursors to P wave arrivals in New Zealand: implications for slab structure, *J. geophys. Res.,* **101**(B4), 8473–8488.

Walcott, R.I., 1978. Present tectonics and late Cenozoic evolution of New Zealand, *Geophys. J. R. astr. Soc.,* **52,** 137–164.

Walcott, R.I., 1987. Geodetic strain and the deformational history of the North Island of New Zealand during the late Cainozoic, *Phil. Trans. R. Soc. Lond.,* A, **321,** 163–181.